Surface acoustic wave coupled to magnetic resonance on multiferroic CuB_2O_4

R. Sasaki,[1] Y. Nii,[2] and Y. Onose[2]
[1]*Department of Basic Science, University of Tokyo, Tokyo 153-8902, Japan*
[2]*Institute for Materials Research, Tohoku University, Sendai 980-8577, Japan*

(Received 5 November 2018; published 18 January 2019)

We observed surface acoustic wave (SAW) propagation on a multiferroic material CuB_2O_4 with use of two interdigital transducers (IDTs). The period of IDT fingers is as short as 1.6 μm so that the frequency of SAW is 3 GHz, which is comparable with that of magnetic resonance. In the antiferromagnetic phase, the SAW excitation intensity varied with the magnitude and direction of the magnetic field, owing to the dynamical coupling between SAWs and antiferromagnetic resonance of CuB_2O_4. The microscopic mechanism is discussed based on the symmetrically allowed magnetoelastic coupling.

DOI: 10.1103/PhysRevB.99.014418

I. INTRODUCTION

Multiferroics are materials where magnetism and ferroelectricity coexist. Novel electromagnetic phenomena are frequently observed, thanks to the interplay between the magnetism and ferroelectricity. For example, they show giant magnetoelectric effects, which is polarization change induced by a magnetic field, and reciprocally magnetization change induced by an electric field [1,2]. The interplay is valid even for the dynamical state. The magnetoelectric correlation in the optical frequency range gives rise to nonreciprocal directional dichroism [3–5]. The electric-field active magnon mode has also been observed in multiferroics [6]. Here, we study the dynamical coupling between an antiferromagnetic magnon and a surface acoustic wave (SAW) in a multiferroic CuB_2O_4.

The SAW is an elastic wave localized on a surface of media [7]. The amplitude decays exponentially with the depth from the surface. The SAW can be excited and detected on a piezoelectric substrate with use of interdigital transducers (IDTs). The SAW can carry electromagnetic signals between two separated IDTs when the wavelength coincides with the IDT finger period. The SAW devices composed of two IDTs on a piezoelectric substrate are industrially used as bandpass filters or delay lines. The combination with magnetism seems useful for making these devices more functional. In fact, introducing ferromagnetic thin film between two IDTs gives rise to emergent functionality such as acoustically driven ferromagnetic resonance [8–10], acoustic spin pumping [11,12], and nonreciprocal SAW propagation [13]. A more direct way of introducing magnetism is replacing a piezoelectric substrate with a multiferroic one. Quite recently, we succeeded in fabricating a SAW device based on a multiferroic material $BiFeO_3$ in collaboration with other researchers [14]. We observed that the SAW intensity and velocity were modulated due to the static magnetostructural change in the magnetic fields. One might think the dynamical coupling between a SAW and a magnon should show more rich phenomena but the magnon mode in $BiFeO_3$ is too high to be coupled to a SAW [15,16]. In order to elucidate this issue, we investigate a SAW coupled to a magnon mode on another multiferroic material CuB_2O_4.

CuB_2O_4 has the noncentrosymmetric but nonpolar crystal structure with a space group of $I\bar{4}2d$. According to symmetry analysis, the piezoelectric tensor is expressed as

$$\begin{pmatrix} 0 & 0 & 0 & d_1 & 0 & 0 \\ 0 & 0 & 0 & 0 & d_1 & 0 \\ 0 & 0 & 0 & 0 & 0 & d_2 \end{pmatrix}, \quad (1)$$

where d_1 and d_2 are nonvanishing constants. As discussed later, the SAW can be generated in some choice of the device plane and propagation direction. At low temperature, CuB_2O_4 exhibits two successive magnetic phase transitions at $T_N = 21$ K and $T^* = 9$ K. Below T_N, it shows easy-plane Néel-type antiferromagnetic order [17]. Ferroelectric polarization depending on the direction of antiferromagnetic moments is emergent in this magnetic phase. Several unusual optical phenomena have been reported such as magnetic field induced second-harmonic generation [18] and magneto-optical dichroism [4]. The second transition at 9 K corresponds to the incommensurate helical ordering. In these magnetic states, a magnetic resonance mode was observed in the low-frequency range of several GHz [19–21], owing to the small magnetic anisotropy of the Cu^{2+} $S = 1/2$ moment. The SAW excitation in this frequency range can be achieved by means of the conventional electron-beam lithography technique. Therefore, this material is suitable for the investigation of the SAW coupled to the magnetic resonance.

II. SAW DEVICE AND EXCITATION

We fabricated a SAW device on CuB_2O_4 substrate [Fig. 1(a)]. The CuB_2O_4 single crystal was synthesized by the flux method [22]. Two Al IDTs with a thickness of 50 nm were fabricated on the substrate using electron-beam lithography and electron-beam evaporation. One finger width of the IDT and space between the fingers were designed to be 400 nm [Fig. 1(b)] so that the center wavelength of SAWs is 1.6 μm, which is determined by the periodicity of IDTs. The number of the finger pair of IDTs is 50. The distance between the center of the two IDTs is 580 μm. We designed the CuB_2O_4 SAW device so that the surface of the substrate is perpendicular to the crystal [001] axis, and the SAW propagation direction is parallel to the [110] axis

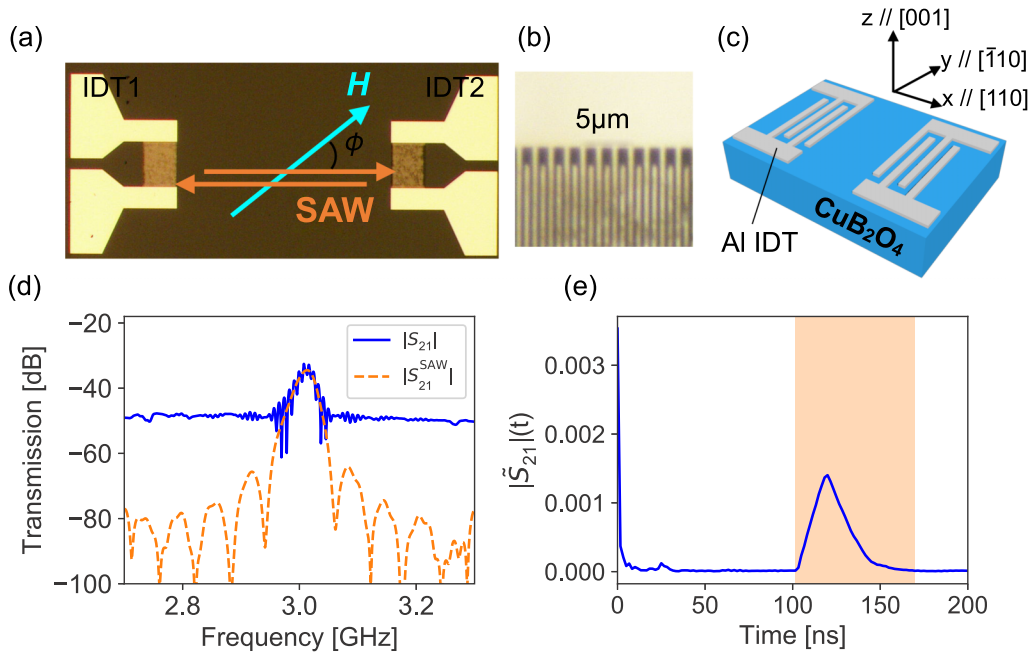

FIG. 1. (a) Top view of CuB_2O_4 SAW device used in this research. Magnetic field was applied along the surface of the device. (b) Enlarged view of Al IDT. (c) Schematic diagrams of the device. the surface of device is (001) plane of the CuB_2O_4 crystal, and SAW propagation direction is parallel to the [110] axis. (d) Transmission between two IDTs. Solid line is the raw data measured and dashed line shows the transmission due to SAW deduced by the Fourier transformation analysis (see text). (e) Transmission as a function of time obtained by the inverse Fourier transformation. Data in the colored region are used for the Fourier transformation to the SAW transmission S_{21}^{SAW}.

[Fig. 1(c)]. When the x, y, z coordinate is defined as $x||[110]$, $y||[\bar{1}10]$, and $z||[001]$, alternating electric field induced on the IDT has x and z components, and the Rayleigh-type SAW has $\epsilon_{xx}, \epsilon_{zz}, \epsilon_{zx}$ components of strain tensor ϵ_{ij} [7]. In this coordinate system, the piezoelectric tensor can be described as

$$\frac{1}{2}\begin{pmatrix} 0 & 0 & 0 & 0 & 2d_1 & 0 \\ 0 & 0 & 0 & -2d_1 & 0 & 0 \\ d_2 & -d_2 & 0 & 0 & 0 & 0 \end{pmatrix}. \tag{2}$$

Because $\epsilon_{xx}, \epsilon_{zx}$ components can be induced by the IDT electric field, the SAW can be excited in this configuration. All the measurements were performed at $T = 10$ K. As shown in Fig. 1(a), the magnetic field is applied parallel to the device surface, and the azimuth angle of the magnetic field from the SAW propagation direction is defined as ϕ.

Figure 1(d) shows the absolute value of complex forward transmission from left IDT (IDT 1) to right IDT (IDT 2) $[|S_{21}|(f)]$ measured by a vector network analyzer (Agilent E5071C). We have found a broad peak with small ripples around 3 GHz. In order to confirm that this is the SAW signal, we perform a time-domain analysis. Figure 1(e) shows the absolute value of time domain complex transmission $\tilde{S}_{21}(t)$ obtained by an inverse Fourier transformation [23]:

$$\tilde{S}_{21}(t) = \frac{1}{N}\sum_{k=1}^{N} |S_{21}|(f_k)\exp[\angle S_{21}(f_k)]e^{2\pi i f_k t}, \tag{3}$$

where N, t, f_k, and $\angle S_{21}(f)$ are the number of observed data, time, kth frequency ($k = 1, \ldots, N$), and phase delay of transmission in the frequency domain. The large impulse observed around 0 ns is due to the direct electromagnetic transmission between two IDTs. In addition, we have observed the delayed impulse around 120 ns. From the distance between IDTs, the velocity of the delayed transmission signal is estimated as 4.8×10^3 m/s, which almost coincides with the phase velocity estimated from the frequency and IDT finger period. Because the velocity is comparable with the SAW velocity of other piezoelectrics (e.g., 3488 m/s for YZ-cut $LiNbO_3$ [7]), the delayed signal can be attributed to the SAW signal. We obtained the absolute value of SAW transmission spectra $|S_{21}^{\mathrm{SAW}}|(f)$ by performing Fourier transformation of the complex $\tilde{S}_{21}(t)$ only on the SAW transmission time region [the colored region in Fig. 1(e)]. In this spectrum, the ripples are removed, and the background level is decreased. Hereafter, we used the $|S_{21}^{\mathrm{SAW}}|(f)$ spectra for the analysis of the SAW transmission (for the reflection S_{11}, we performed another analysis as discussed later).

III. MAGNON-SAW COUPLING

Figure 2(a) shows the magnetic field dependence of microwave absorption spectra at $T = 10$ K. It is measured in the measurement system for conventional microwave spectroscopy with a coplanar waveguide, which is used for the previous study [21]. The static and alternating magnetic fields were parallel to the [110] axis and (110) plane, respectively. We have found a magnetic resonance mode in this frequency region. The frequency increases almost linearly with the magnetic field. As discussed in Appendix D, the origin is ascribed to the acoustic mode of antiferromagnetic resonance. Figure 2(b) shows the magnetic field dependence of microwave absorption at 3.013 GHz, which is the peak frequency

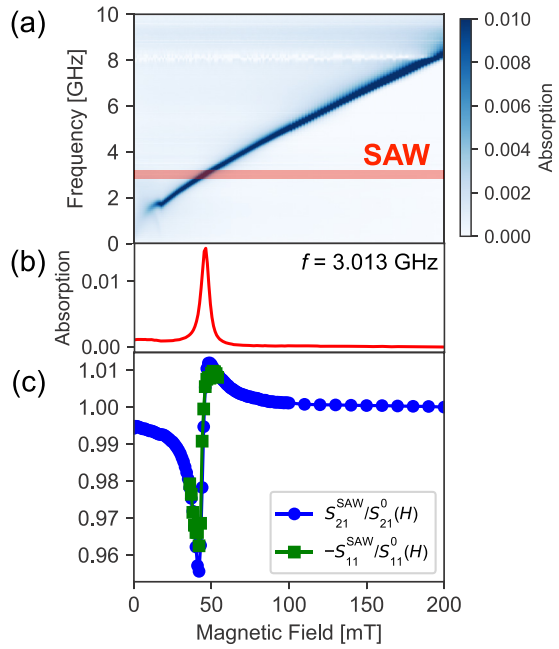

FIG. 2. (a) Magnetic field dependence of microwave absorption due to magnetic resonance of CuB_2O_4. The external magnetic field is parallel to [110] axis. Thick line shows the SAW frequency. (b) Magnetic field dependence of microwave absorption at 3.013 GHz due to magnetic resonance. (c) Magnetic field dependence of normalized SAW transmission S_{21}^{SAW}/S_{21}^{0} and excitation $-S_{11}^{SAW}/S_{11}^{0}$.

of SAW transmission $|S_{21}^{SAW}|(f)$ in Fig. 1(d). The magnetic resonance frequency coincided with the frequency of the SAW around 46 mT.

Figure 2(c) shows magnetic field dependence of SAW transmission normalized by that at 200 mT, where the magnetic resonance frequency is far above the SAW frequency $[S_{21}^{SAW}/S_{21}^{0}(H)$; for the precise definition, see Appendix A]. The SAW transmission gradually decreases with increasing magnetic field from 0 mT. It shows rapid increase when the magnetic resonance frequency coincides with the SAW frequency. Then it decreases toward the high field. While the SAW frequency doesn't vary with the magnetic field and the signature of energy-level anticrossing was not observed, this characteristic magnetic field dependence seems caused by the interaction between the SAW and magnetic resonance. In Fig. 2(c), we also plotted SAW excitation intensity at IDT 1 normalized by the 200 mT value $[-S_{11}^{SAW}/S_{11}^{0}(H)$; for the precise definition, see Appendix A], which is estimated by the decrease of reflection due to SAW generation. Because both the transmission and excitation show similar dependence on the magnetic field, it seems that the magnetic field dependence is caused by the excitation process.

In order to discuss the microscopic origin of magnetic field dependence, we show the SAW transmission as a function of the magnetic field along various directions ϕ in Fig. 3(a). The magnetic field dependence became broad and the magnitude decreased with increasing or decreasing ϕ from 0°. Nevertheless, the characteristic magnetic field dependence around 40 mT was still discerned even at $\phi = \pm 90°$. Irrespective of the field angle, the magnetic field dependence is almost unchanged when the field direction or propagation direction

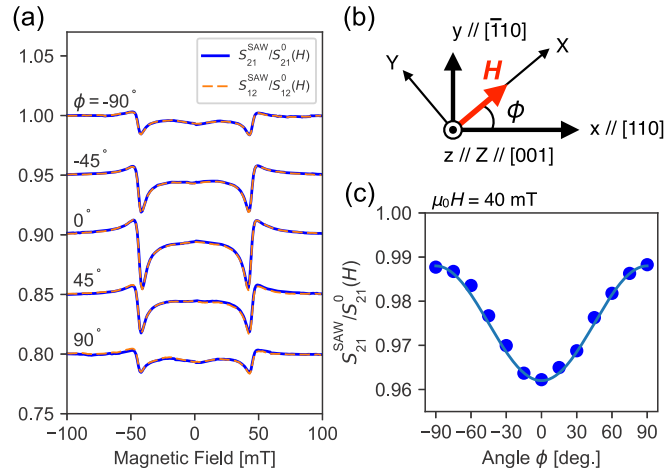

FIG. 3. (a) Normalized SAW transmissions S_{21}^{SAW} and S_{12}^{SAW} as a function of magnetic fields with various directions. Solid lines show the transmission from port 1 to port 2 (S_{21}^{SAW}/S_{21}^{0}) and dashed lines are transmission for opposite direction (S_{12}^{SAW}/S_{12}^{0}). (b) Illustration of xyz- and XYZ-coordinate systems. (c) Magnetic field angle dependence of normalized SAW transmission S_{21}^{SAW} at $\mu_0 H = 40$ mT. Solid line shows $C_1 - C_2 \cos^2\phi$.

is reversed $[S_{12}^{SAW}/S_{12}^{0}(H)$ is the normalized transmission for the opposite SAW propagation direction]. Figure 3(c) shows the magnetic field angle dependence of SAW transmission at 40 mT. The SAW transmission varied with ϕ as $C_1 - C_2 \cos^2\phi$ (C_1 and C_2 are constants).

Let us theoretically discuss the microscopic origin of the magnetic field dependence of the SAW signal. The observed magnetic field dependence in Fig. 2(c) seems the function of $(\omega_{Mag} - \omega_{SAW})^{-1}$, where ω_{Mag} is the magnetic resonance frequency almost proportional to the magnetic field and ω_{SAW} is the magnetic field independent frequency of SAW. When ω_{Mag} is increased from 0, the magnitude of negative magnetic field dependent part increases. It shows steep sign change at $\omega_{Mag} = \omega_{SAW}$ and then decreases. This type of factor is frequently seen in two mode coupled phenomena because the hybridized strength is proportional to this factor. Therefore the magnetic field variation of SAW excitation should be caused by the magnon-SAW coupling although the complete microscopic understanding is not obtained at present. The angle dependence [Fig. 3(c)] is more closely related to the microscopic mechanism. To discuss this issue we should consider the explicit form of magnetoelastic coupling. The magnetoelastic coupling energy in antiferromagnetic ordered state is

$$F_{me} = \sum_{p,q=1,2} \sum_{i,j,k,l=1,2,3} b_{pqijkl} m_{pi} m_{qj} \epsilon_{kl}, \qquad (4)$$

where m_{pi} represents the i component of magnetization on p sublattice of the antiferromagnet, and ϵ_{kl} is the strain tensor on the surface of the device. The subscripts 1,2,3 for i, j, k, l indicate x, y, z components, respectively. The coefficients b_{pqijkl} represent magnetoelastic coupling constants. The nonvanishing component of b_{pqijkl} is determined by the symmetry analysis (see Appendix B). The effective magnetic field $\boldsymbol{h}_p^{me}$ due to the strains acting on the magnetic

moments at p-sublattice $\boldsymbol{m}_p$ is given by $\boldsymbol{h}_p^{me} = -\nabla_{\boldsymbol{m}_p} F_{me}$. To understand the acoustic antiferromagnetic resonance under SAW excitation, we consider Landau-Lifshitz (LL) equation without a damping term, in which the magnetic moments are driven by $\boldsymbol{h}_p^{me}$ as well as $\boldsymbol{H}$ and anisotropy field. By partially diagonalizing six components of the equation, we can deduce three effective equations regarding the acoustic antiferromagnetic resonance as follows (see Appendix C):

$$\frac{1}{\gamma}\frac{\partial}{\partial t}\left((\delta m_{1X} - \delta m_{2X}) + \frac{b}{a^2}(\delta m_{1Y} + \delta m_{2Y})\right) = (m^0)^2\left(B_1 + \frac{b}{a^2}B_2\right)\epsilon_{31}\cos\phi, \tag{5}$$

$$\left(\frac{1}{\gamma}\frac{\partial}{\partial t} - iaH^0\right)[(\delta m_{1Y} + \delta m_{2Y}) + ia(\delta m_{1Z} + \delta m_{2Z})] = (m^0)^2(B_2\epsilon_{31}\cos\phi + iaB_3\epsilon_{11}\sin 2\phi), \tag{6}$$

$$\left(\frac{1}{\gamma}\frac{\partial}{\partial t} + iaH^0\right)[(\delta m_{1Y} + \delta m_{2Y}) - ia(\delta m_{1Z} + \delta m_{2Z})] = (m^0)^2(B_2\epsilon_{31}\cos\phi - iaB_3\epsilon_{11}\sin 2\phi). \tag{7}$$

Here, γ and H^0 are the gyromagnetic ratio and the magnitude of the external magnetic field, respectively. $\delta\boldsymbol{m}_p$ and m^0 are defined by $\delta\boldsymbol{m}_p = \boldsymbol{m}_p - \boldsymbol{m}_p^0$ and $m^0 = |\boldsymbol{m}_p^0|$, where $\boldsymbol{m}_p^0$ is static part of magnetic moments. The XYZ coordinate system is defined as in Fig. 3(b), so that the X axis is parallel to the magnetic field. Dimensionless constants a and b are defined by $a = \sqrt{(-\frac{K}{m^0}\cos\psi + H^0)/H^0}$ and $b = (-\frac{K}{m^0} + 2m^0\Lambda)\sin\psi/H^0$, where K, Λ, and ψ are the uniaxial magnetic anisotropy constant, molecular field constant, and angle between the sublattice magnetic moments and magnetic field, respectively. B_1, B_2, and B_3 are constants defined by

$$B_1 = 8\sin\psi[(b_{111313} + b_{121313})\cos\psi - b_{121323}\sin\psi], \tag{8}$$

$$B_2 = -8\cos\psi[(b_{111313} + b_{121313})\cos\psi - b_{121323}\sin\psi], \tag{9}$$

$$B_3 = -2[(b_{111111} - b_{111122})\cos 2\psi + b_{121111} - b_{121122}]. \tag{10}$$

In the absence of SAW excitation, the right-hand sides of Eqs. (5)–(7) vanish. In this case, these equations stand for the pure antiferromagnetic excitation. Because $\omega_{\mathrm{Mag}} > 0$, only right-hand ellipsoidal polarized components $(\delta m_{1Y} + \delta m_{2Y}) + ia(\delta m_{1Z} + \delta m_{2Z})$ exhibit resonance behavior at $\omega_{\mathrm{Mag}} = \gamma a H^0$. Equation (7) does not show any resonance behavior, and Eq. (5) stand for the constraint condition describing the relationship between magnetic-moment components parallel $(\delta m_{1X}, \delta m_{2X})$ and perpendicular $(\delta m_{1Y}, \delta m_{2Y})$ to the magnetic field during the precession motion of magnetic moments. The right-hand sides of these equations are the magnetic torque due to the SAW excitation. In particular, the right-hand side of Eq. (6) is the direct coupling between the SAW and magnetic resonance mode. The magnitude of magnon-SAW coupling is proportional to

$$|B_2\epsilon_{31}\cos\phi + iaB_3\epsilon_{11}\sin 2\phi|^2. \tag{11}$$

The experimentally obtained magnetic field angle dependence of normalized SAW transmission $C_1 - C_2\cos^2\phi$ shown in Fig. 3(c) seems to reflect the first term. The second term seems to be negligible, which is composed of longitudinal-type magnetoelastic coupling constants. Therefore, it seems that the strain ϵ_{31} most effectively excites the acoustic antiferromagnetic resonance. Note that nonreciprocity should be caused by the mixture of phase different effective magnetic fields induced by the shear-type and longitudinal acoustic strains, similarly to the case of Ni/$LiNbO_3$ [13]. In this case, however, the longitudinal-type magnetoelastic coupling is absent, and the magnetic field is linearly polarized. That is why the nonreciprocity is negligible in this system. The constant term C_1 cannot be deduced by the present theoretical analysis, in which the magnitude of magnetic moments is fixed. Perhaps, the constant term is caused by the magnetic field change of the magnitude.

IV. CONCLUSION

In conclusion, we could successfully excite and detect the surface acoustic wave on multiferroic material CuB_2O_4 by fabricating the interdigital transducers on a CuB_2O_4 single-crystal substrate. In the antiferromagnetic phase, SAW excitation and transmission exhibited characteristic change due to the coupling to the antiferromagnetic resonance. This magnetic field angle dependence was explained by the analysis using the effective magnetic field caused by magnetoelastic coupling. While the magnitude of magnetic field variation is still comparable with those reported in previous research [8–13], this work may pave a different path to increase the controllability of the SAW device based on multiferroic materials.

ACKNOWLEDGMENT

This work was supported in part by the Grant-in-Aid for Scientific Research (Grants No. 17H05176 and No. 16H04008) and for Young Scientists (Grant No. 18K13494) from the Japan Society for the Promotion of Science and the Noguchi Institute. R.S. was supported by the Grant-in-Aid for JSPS Research Fellow (Grant No. 18J12130).

APPENDIX A: DEFINITIONS OF RELATIVE SAW EXCITATION AND TRANSMISSION $-S_{11}^{\mathrm{SAW}}/S_{11}^0(H)$ AND $S_{21}^{\mathrm{SAW}}/S_{21}^0(H)$

Figure 4(a) shows reflection of the device $|S_{11}|(f)$ under the external magnetic fields $\mu_0 H = 40$, 45, 50, and 200 mT. The external magnetic field is applied parallel to the SAW propagation direction, i.e., $\phi = 0°$. There are three components of decrease of reflection (absorption); a sharp dip, broad dip, and background signal from the device. Three sharp spikes seen between 2.75 and 3.00 GHz are noise due to the interference with the small reflected microwave from some part of measurement circuit. While the sharp dip and background do not show large magnetic field variation, the frequency of broad dip increases with the magnetic field. Therefore, we ascribed the origins of sharp and broad dips to SAW and magnetic resonance, respectively. In order to accurately estimate

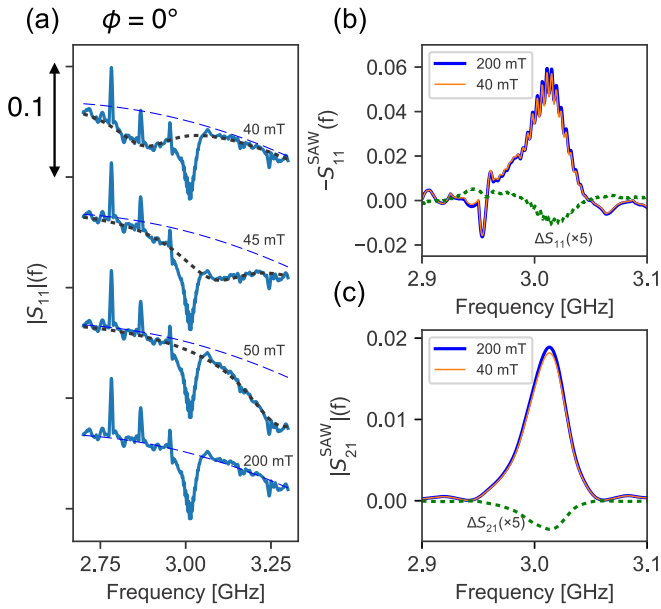

FIG. 4. (a) Microwave reflection from the SAW device $|S_{11}|(f)$ at several magnetic fields. The magnetic fields are applied parallel to the SAW propagation direction. The solid line shows the observed data, and the dotted and dashed lines are the result of fitting of magnetic resonance and background, respectively (see text). (b) SAW excitation $-S_{11}^{SAW}$ at 40 and 200 mT and the difference between 40- and 200-mT values (ΔS_{11}). (c) SAW transmission S_{21}^{SAW} at 40 and 200 mT and their difference (ΔS_{21}). ΔS_{11} and ΔS_{21} in (b) and (c) are multiplied by 5.

the SAW contribution, we fitted the contribution of magnetic resonance and background to the Lorentzian and quadratic function, respectively, and subtract them from $|S_{11}|(f)$. Figure 4(b) shows the minus subtracted reflection $-S_{11}^{SAW}(f)$ at $\mu_0 H = 40$ and 200 mT. Because the frequency of magnetic resonance is far above 3 GHz at 200 mT, the SAW excitation is not affected by the magnetic resonance. When the magnetic field is decreased to 40 mT, the SAW intensity decreases [Fig. 4(b)]. Similarly, the transmission at 40 mT is a little smaller than that at 200 mT as shown in Fig. 4(c). The relative change of SAW excitation and transmission is defined as

$$-S_{11}^{SAW}/S_{11}^{0}(H) = -\max\{|S_{11}^{SAW}|(f)\}(H)/\max\{|S_{11}^{SAW}|(f)\}(200\ \text{mT}/\mu_0), \tag{A1}$$

$$S_{21}^{SAW}/S_{21}^{0}(H) = \max\{|S_{21}^{SAW}|(f)\}(H)/\max\{|S_{21}^{SAW}|(f)\}(200\ \text{mT}/\mu_0), \tag{A2}$$

where max{} stands for the maximum value. These quantities are plotted in Fig. 2(c) in the main text.

APPENDIX B: MAGNETOELASTIC COUPLING ENERGY

As discussed above, the magnetoelastic coupling energy in the staggered antiferromagnetic state can be expressed as

$$F_{me} = \sum_{p,q=1,2} \sum_{i,j,k,l=1,2,3} b_{pqijkl} m_{pi} m_{qj} \epsilon_{kl}. \tag{B1}$$

Because the magnetoelastic coupling energy is unchanged by the symmetry operation belong to the space group $I\bar{4}2d$, some of constants b_{pqijkl} should vanish and the number of independent magnetoelastic coupling constants decrease. The reduced magnetoelastic coupling energy can be represented by the following equation:

$$\begin{aligned}
F_{me} = {} & \epsilon_{11}\big[b_{111111}m_{11}^2 + 2b_{121111}m_{21}m_{11} + b_{111111}m_{21}^2 + b_{111122}\big(m_{12}^2 + m_{22}^2\big) + b_{113311}\big(m_{13}^2 + m_{23}^2\big) \\
& + 2b_{121122}m_{12}m_{22} + 2b_{121211}(m_{11}m_{22} - m_{12}m_{21}) + 2b_{123311}m_{13}m_{23}\big] \\
& + \epsilon_{12}[4b_{111212}(m_{11}m_{12} + m_{21}m_{22}) + 4b_{121212}(m_{12}m_{21} + m_{11}m_{22})] \\
& + \epsilon_{13}\{4[m_{21}(b_{111313}m_{23} + b_{121313}m_{13}) + m_{11}(b_{111313}m_{13} + b_{121313}m_{23}) \\
& + b_{121323}(m_{13}m_{22} - m_{12}m_{23})]\} \\
& + \epsilon_{22}\big[b_{111111}m_{12}^2 + 2b_{121111}m_{22}m_{12} + b_{111111}m_{22}^2 + b_{111122}\big(m_{11}^2 + m_{21}^2\big) \\
& + b_{113311}\big(m_{13}^2 + m_{23}^2\big) + 2b_{121122}m_{11}m_{21} + 2b_{121211}(m_{11}m_{22} - m_{12}m_{21}) + 2b_{123311}m_{13}m_{23}\big] \\
& + \epsilon_{23}\{4[m_{22}(b_{111313}m_{23} + b_{121313}m_{13}) + m_{12}(b_{111313}m_{13} + b_{121313}m_{23}) \\
& + b_{121323}(m_{11}m_{23} - m_{13}m_{21})]\} \\
& + \epsilon_{33}\big[b_{111133}m_{11}^2 + 2m_{11}(b_{121133}m_{21} + b_{121233}m_{22}) + b_{111133}m_{12}^2 + b_{111133}\big(m_{21}^2 + m_{22}^2\big) \\
& + b_{113333}\big(m_{13}^2 + m_{23}^2\big) + 2m_{12}(b_{121133}m_{22} - b_{121233}m_{21}) + 2b_{123333}m_{13}m_{23}\big].
\end{aligned} \tag{B2}$$

APPENDIX C: EFFECTIVE EQUATIONS OF MOTION FOR THE ANTIFERROMAGNETIC RESONANCES UNDER THE SAW EXCITATIONS

The effective magnetic field on the magnetization $\boldsymbol{m}_p$ $(p = 1, 2)$ is defined by

$$\boldsymbol{h}_p^{me} = -\nabla_{\boldsymbol{m}_p} F_{me} = \big(h_{p1}^{me}, h_{p2}^{me}, h_{p3}^{me}\big). \tag{C1}$$

The subscript p represents the index of two sublattices of ordered spins.

Assuming that $\boldsymbol{h}_p^{me}$ acts on the magnetic moments similarly to the real magnetic field, the LL equation without a damping term is represented by

$$\frac{\partial \boldsymbol{m}_p}{\partial t} = -\gamma \boldsymbol{m}_p \times \left\{ -\Lambda \boldsymbol{m}_q + \frac{K}{|\boldsymbol{m}_p|^2}(\boldsymbol{m}_p \cdot \hat{z})\hat{z} + \boldsymbol{h}_p^{me} + \boldsymbol{H} \right\}, \tag{C2}$$

where $\hat{z}$ is the unit vector along the z axis. By putting $\boldsymbol{m}_p = \boldsymbol{m}_p^0 + \delta \boldsymbol{m}_p$ and linearizing the six equations with respect to $\delta \boldsymbol{m}$ and $\boldsymbol{h}_p^{me}$, we get

$$\frac{1}{\gamma}\frac{\partial \delta \boldsymbol{m}_p}{\partial t} + \boldsymbol{m}_p^0 \times \left(-\Lambda \delta \boldsymbol{m}_q + \frac{K}{(m^0)^2}(\delta \boldsymbol{m}_p \cdot \hat{z})\hat{z} \right) + \delta \boldsymbol{m}_p \times \left(-\Lambda \boldsymbol{m}_q^0 + \boldsymbol{H} \right) = -\boldsymbol{m}_p^0 \times \boldsymbol{h}_p^{me}, \tag{C3}$$

where $p, q = 1$ or 2 and $p \neq q$.

Based on the reduced magnetoelastic coupling energy (B2), the effective magnetic field components form

$$\begin{aligned}
h_{11}^{me} &= -2m_{11}^0(b_{111111}\epsilon_{11} + b_{111122}\epsilon_{22} + b_{111133}\epsilon_{33}) - 2m_{21}^0(b_{121111}\epsilon_{11} + b_{121122}\epsilon_{22} + b_{121133}\epsilon_{33}) \\
&\quad - 2m_{22}^0[b_{121211}(\epsilon_{11} + \epsilon_{22}) + 2b_{121212}\epsilon_{12} + b_{121233}\epsilon_{33}] - 4b_{111212}m_{12}^0\epsilon_{12}, \\
h_{12}^{me} &= -2b_{111111}m_{12}^0\epsilon_{22} - 2b_{111122}m_{12}^0\epsilon_{11} - 2b_{111133}m_{12}^0\epsilon_{33} - 4b_{111212}m_{11}^0\epsilon_{12} - 2b_{121111}m_{22}^0\epsilon_{22} \\
&\quad - 2b_{121122}m_{22}^0\epsilon_{11} - 2b_{121133}m_{22}^0\epsilon_{33} + 2m_{21}^0[b_{121211}(\epsilon_{11} + \epsilon_{22}) - 2b_{121212}\epsilon_{12} + b_{121233}\epsilon_{33}], \\
h_{13}^{me} &= -4b_{111313}m_{11}^0\epsilon_{31} - 4b_{111313}m_{12}^0\epsilon_{23} - 4b_{121313}m_{22}^0\epsilon_{23} - 4b_{121323}m_{22}^0\epsilon_{31} \\
&\quad + 4m_{21}^0(b_{121323}\epsilon_{23} - b_{121313}\epsilon_{31}), \\
h_{21}^{me} &= -2m_{21}^0(b_{111111}\epsilon_{11} + b_{111122}\epsilon_{22} + b_{111133}\epsilon_{33}) - 2m_{11}^0(b_{121111}\epsilon_{11} + b_{121122}\epsilon_{22} + b_{121133}\epsilon_{33}) \\
&\quad + 2m_{12}^0[b_{121211}(\epsilon_{11} + \epsilon_{22}) - 2b_{121212}\epsilon_{12} + b_{121233}\epsilon_{33}] - 4b_{111212}m_{22}^0\epsilon_{12}, \\
h_{22}^{me} &= -2b_{111111}m_{22}^0\epsilon_{22} - 2b_{111122}m_{22}^0\epsilon_{11} - 2b_{111133}m_{22}^0\epsilon_{33} - 4b_{111212}m_{21}^0\epsilon_{12} - 2b_{121111}m_{12}^0\epsilon_{22} \\
&\quad - 2b_{121122}m_{12}^0\epsilon_{11} - 2b_{121133}m_{12}^0\epsilon_{33} - 2m_{11}^0[b_{121211}(\epsilon_{11} + \epsilon_{22}) + 2b_{121212}\epsilon_{12} + b_{121233}\epsilon_{33}], \\
h_{23}^{me} &= -4b_{111313}m_{21}^0\epsilon_{31} - 4b_{111313}m_{22}^0\epsilon_{23} - 4b_{121313}m_{12}^0\epsilon_{23} + 4b_{121323}m_{12}^0\epsilon_{31} \\
&\quad - 4m_{11}^0(b_{121313}\epsilon_{31} + b_{121323}\epsilon_{23}).
\end{aligned} \tag{C4}$$

Here we estimate the effective magnetic field due to the small strain. Therefore, we neglect the dynamical component of magnetization ($\delta \boldsymbol{m}_p$). Since the magnetic order in CuB_2O_4 at $T = 10$ K is easy-plane Néel-type magnetic order, we assume $m_{p3}^0 = 0$.

From the fact that the device was designed so that its sagittal plane is parallel to the mirror plane of the crystal, we can assume that the Rayleigh-type SAW mode is excited in our measurement [24]. We neglected the strain components other than ϵ_{11}, ϵ_{33}, and ϵ_{31}, of which the Rayleigh-type SAW is composed. By diagonalizing Eq. (C3), we get the six equations for antiferromagnetic resonance as follows:

$$\frac{1}{\gamma}\frac{\partial}{\partial t}\left((\delta m_{1X} - \delta m_{2X}) + \frac{b}{a^2}(\delta m_{1Y} + \delta m_{2Y}) \right) = (m^0)^2 \left(B_1 + \frac{b}{a^2}B_2 \right)\epsilon_{31}\cos\phi, \tag{C5}$$

$$\left(\frac{1}{\gamma}\frac{\partial}{\partial t} - iaH^0 \right)[(\delta m_{1Y} + \delta m_{2Y}) + ia(\delta m_{1Z} + \delta m_{2Z})] = (m^0)^2(B_2\epsilon_{31}\cos\phi + iaB_3\epsilon_{11}\sin 2\phi), \tag{C6}$$

$$\left(\frac{1}{\gamma}\frac{\partial}{\partial t} + iaH^0 \right)[(\delta m_{1Y} + \delta m_{2Y}) - ia(\delta m_{1Z} + \delta m_{2Z})] = (m^0)^2(B_2\epsilon_{31}\cos\phi - iaB_3\epsilon_{11}\sin 2\phi), \tag{C7}$$

$$\frac{1}{\gamma}\frac{\partial}{\partial t}[(\delta m_{1X} + \delta m_{2X}) + c(\delta m_{1Y} - \delta m_{2Y})] = (m^0)^2(B_4 + cB_5)\epsilon_{13}\cos\phi, \tag{C8}$$

$$\begin{aligned}
&\left(\frac{1}{\gamma}\frac{\partial}{\partial t} - ie(2m\Lambda\cos\psi - H^0) \right)[d(\delta m_{1X} + \delta m_{2X}) + (\delta m_{1Y} - \delta m_{2Y}) - ie(\delta m_{1Z} - \delta m_{2Z})] \\
&= (m^0)^2(dB_4 + B_5)\epsilon_{13}\cos\phi - ie[B_6\epsilon_{33} + \epsilon_{11}(B_7\cos 2\phi + B_8)],
\end{aligned} \tag{C9}$$

$$\begin{aligned}
&\left(\frac{1}{\gamma}\frac{\partial}{\partial t} + ie(2m\Lambda\cos\psi - H^0) \right)[d(\delta m_{1X} + \delta m_{2X}) + (\delta m_{1Y} - \delta m_{2Y}) + ie(\delta m_{1Z} - \delta m_{2Z})] \\
&= (m^0)^2(dB_4 + B_5)\epsilon_{13}\cos\phi + ie[B_6\epsilon_{33} + \epsilon_{11}(B_7\cos 2\phi + B_8)],
\end{aligned} \tag{C10}$$

where $\delta m_{1X} = \delta m_{11}\cos\phi + \delta m_{12}\sin\phi$, $\delta m_{2X} = \delta m_{21}\cos\phi + \delta m_{22}\sin\phi$, $\delta m_{1Y} = -\delta m_{11}\sin\phi + \delta m_{12}\cos\phi$, $\delta m_{2Y} = -\delta m_{21}\sin\phi + \delta m_{22}\cos\phi$, $\delta m_{1Z} = \delta m_{13}$, $\delta m_{2Z} = \delta m_{23}$. Dimensionless constants c, d, and e are defined by $c = \frac{K\sin\psi}{[2\Lambda(m^0)^2+K]\cos\psi - m^0 H^0}$, $d = \frac{2m^0\Lambda\sin\psi}{2m^0\Lambda\cos\psi - H^0}$, $e = \frac{\sqrt{(H^0)^2 - [4\Lambda(m^0)+K/m^0]\cos\psi H^0 + 2\Lambda\{\Lambda(m^0)^2+[\Lambda(m^0)^2+K]\cos 2\psi\}}}{2m^0\Lambda\cos\psi - H^0}$. B_4, B_5, and B_6 are constants defined by

$$B_4 = 8\sin\psi[(b_{121313} - b_{111313})\sin\psi + b_{121323}\cos\psi], \tag{C11}$$

$$B_5 = -8\cos\psi[(b_{121313} - b_{111313})\sin\psi + b_{121323}\cos\psi], \tag{C12}$$

$$B_6 = -4(b_{121133}\sin 2\psi + b_{121233}\cos 2\psi), \tag{C13}$$

$$B_7 = -2\sin 2\psi(b_{111111} - b_{111122}), \tag{C14}$$

$$B_8 = -2[(b_{121111} + b_{121122})\sin 2\psi + 2b_{121211}\cos 2\psi]. \tag{C15}$$

Equations (C5)–(C7) and (C8)–(C10) are relevant to the acoustic mode and optical mode of antiferromagnetic resonance, respectively.

APPENDIX D: ANTIFERROMAGNETIC RESONANCE MEASUREMENTS

We measured the microwave absorption of CuB_2O_4 in order to study the origin of magnetic resonance. While the magnetic field is along the (001) plane in the previous work [21], it is within the $(1\bar{1}0)$ plane in the present study. The other experimental configurations are similar to those in the previous study. Figure 5 shows microwave absorption in magnetic fields with various directions and the fixed magnitude of 40 mT. θ is defined as the angle between the [001] axis and the magnetic field. As the angle θ decreases, magnetic resonance spectra are shifted to low frequency and their intensity decreases. This is quite consistent with the picture of magnetic resonance in easy-plane antiferromagnets because the lowest magnetic resonance becomes zero mode in the plane-normal magnetic field for the easy-plane antiferromagnets [25]. In the previous work, we tentatively assigned this magnetic resonance to the paramagnetic resonance of the Cu(B) site because this absorption peak is smoothly connected to the magnetic resonance peak above T_N. Nevertheless, this experimental result strongly supports the antiferromagnetic resonance origin.

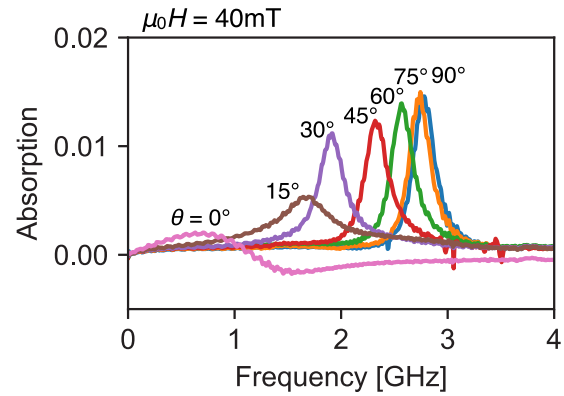

FIG. 5. Microwave absorption spectra in magnetic fields with various directions within the $(1\bar{1}0)$ plane and the fixed magnitude of $\mu_0 H = 40$ mT. θ is defined as the angle between the [001] axis and the magnetic field.

[1] S. W. Cheong and M. Mostovoy, Nat. Mater. **6**, 13 (2007).
[2] Y. Tokura, S. Seki, and N. Nagaosa, Rep. Prog. Phys. Phys. Soc. (Great Britain) **77**, 076501 (2014).
[3] M. Kubota, T. Arima, Y. Kaneko, J. P. He, X. Z. Yu, and Y. Tokura, Phys. Rev. Lett. **92**, 137401 (2004).
[4] M. Saito, K. Ishikawa, K. Taniguchi, and T. Arima, Phys. Rev. Lett. **101**, 117402 (2008).
[5] I. Kézsmárki, N. Kida, H. Murakawa, S. Bordács, Y. Onose, and Y. Tokura, Phys. Rev. Lett. **106**, 057403 (2011).
[6] A. Pimenov, A. A. Mukhin, V. Y. Ivanov, V. D. Travkin, A. M. Balbashov, and A. Loidl, Nat. Phys. **2**, 97 (2006).
[7] D. Morgan, *Surface-wave Devices for Signal Processing*, Studies in Electrical and Electronic Engineering (Elsevier, Amsterdam, 1985).
[8] M. Weiler, L. Dreher, C. Heeg, H. Huebl, R. Gross, M. S. Brandt, and S. T. B. Goennenwein, Phys. Rev. Lett. **106**, 117601 (2011).
[9] L. Dreher, M. Weiler, M. Pernpeintner, H. Huebl, R. Gross, M. S. Brandt, and S. T. B. Goennenwein, Phys. Rev. B **86**, 134415 (2012).
[10] D. Labanowski, A. Jung, and S. Salahuddin, Appl. Phys. Lett. **108**, 022905 (2016).
[11] M. Weiler, H. Huebl, F. S. Goerg, F. D. Czeschka, R. Gross, and S. T. B. Goennenwein, Phys. Rev. Lett. **108**, 176601 (2012).
[12] M. Xu, J. Puebla, F. Auvray, B. Rana, K. Kondou, and Y. Otani, Phys. Rev. B **97**, 180301 (2018).
[13] R. Sasaki, Y. Nii, Y. Iguchi, and Y. Onose, Phys. Rev. B **95**, 020407 (2017).
[14] Y. Ishii, R. Sasaki, Y. Nii, T. Ito, and Y. Onose, Phys. Rev. Appl. **9**, 034034 (2018).
[15] U. Nagel, R. S. Fishman, T. Katuwal, H. Engelkamp, D. Talbayev, H. T. Yi, S.-W. Cheong, and T. Rõõm, Phys. Rev. Lett. **110**, 257201 (2013).
[16] C. Caspers, V. P. Gandhi, A. Magrez, E. de Rijk, and J.-P. Ansermet, Appl. Phys. Lett. **108**, 241109 (2016).
[17] M. Boehm, B. Roessli, J. Schefer, A. S. Wills, B. Ouladdiaf, E. Lelièvre-Berna, U. Staub, and G. A. Petrakovskii, Phys. Rev. B **68**, 024405 (2003).
[18] R. V. Pisarev, I. Sänger, G. A. Petrakovskii, and M. Fiebig, Phys. Rev. Lett. **93**, 037204 (2004).
[19] A. I. Pankrats, G. A. Petrakovskii, and N. V. Volkov, Phys. Solid State **42**, 96 (2000).

[20] T. Fujita, Y. Fujimoto, S. Mitsudo, T. Idehara, K. Inoue, J. Kishine, Y. Kousaka, S. Yano, J. Akimitsu, and M. Motokawa, J. Phys.: Conf. Ser. **51**, 111 (2006).

[21] Y. Nii, R. Sasaki, Y. Iguchi, and Y. Onose, J. Phys. Soc. Jpn. **86**, 024707 (2017).

[22] G. A. Petrakovski, A. I. Pankrats, M. A. Popov, A. D. Balaev, D. A. Velikanov, A. M. Vorotynov, K. A. Sablina, B. Roessli, J. Schefer, A. Amato, U. Staub, M. Boehm, and B. Ouladdiaf, Low Temp. Phys. **28**, 606 (2002).

[23] D. Kobayashi, T. Yoshikawa, M. Matsuo, R. Iguchi, S. Maekawa, E. Saitoh, and Y. Nozaki, Phys. Rev. Lett. **119**, 077202 (2017).

[24] G. W. Farnell and E. L. Adler, in *Physical Acoustics Principles and Methods*, edited by W. P. Mason and R. N. Thurston (Academic, New York, 1972), Vol. 9, p. 35.

[25] A. G. Gurevich and G. A. Melkov, *Magnetization Oscillations and Waves* (CRC Press, Boca Raton, 1996).